CrystEngComm

PAPER

View Article Online
View Journal | View Issue

Cite this: *CrystEngComm*, 2017, **19**, 346

Experimental and theoretical second harmonic generation and photoluminescence from the pseudo-centrosymmetric dihydrochloride salt dihydrate of *trans*-1,2-bis(4-pyridyl)ethene†

Ana Karoline Silva Mendanha Valdo,[a] Cameron Capeletti da Silva,[a] Lauro June Queiroz Maia,[b] Ariel M. Sarotti[c] and Felipe T. Martins*[a]

Received 22nd October 2016,
Accepted 1st December 2016

DOI: 10.1039/c6ce02229d

www.rsc.org/crystengcomm

Here we have prepared a dihydrochloride salt dihydrate of the well-known *trans*-1,2-bis(4-pyridyl)ethene (BPE) featuring both photoluminescent and nonlinear optical properties. In its triclinic lattice (space group *P*1), BPE cations are stacked face-to-tail through π···π interactions between the spacer double-bonded carbons and the protonated pyridyl ring, with a slippage of 3.45 Å always towards the same direction, which is common in other NLO crystals. The existence of inversion symmetry was suggested in its crystal structure, which was ruled out by the SHG emission centred at 487 nm upon excitation at 974 nm. While the fully optimized single molecule of the divalent BPE cation in the gas phase had almost null μ, β_{tot}, β_{CT} and β_{vec} values calculated at the CAM-B3LYP/NLO-V//B3LYP/6-31G* level of theory, these values differed from zero in the crystal conformation. More interestingly, a *ca.* 4-fold increase in β_{tot}, α and μ was observed for the π···π stacked four-molecules as found in its crystal structure. Lastly, this BPE material presents high photoluminescence emission centred at 425 nm under excitation at 366 nm, being therefore a multifunctional optical crystal form.

Introduction

Second order non-linear optical (NLO) properties have been largely investigated in many inorganic and organic materials.[1] Currently, the design and screening of organic materials with NLO efficiency significantly higher than that of inorganic ones are much focused on.[2] There are two main requirements for a crystal form of a molecular compound to exhibit NLO properties. The first is intramolecular, namely, the organic compound should have donor–acceptor π-electron moieties spaced by conjugated bridges, *i.e.*, there is a π-electron delocalization path crossing through the π-electron rich and poor functional groups.[3] Besides having a polarizable π-cloud with electron donating and accepting groups, the second essential feature of such compounds is intermolecular, as they must crystallize without centrosymmetry in the crystal lattice.[4] Such an intermolecular requirement is treated as a challenge in crystal engineering applied to crystalline NLO materials because of their high molecular dipole moment as a consequence of terminal donor and acceptor π-electron moieties. As expected, dipole–dipole interactions are strong in these materials and they do drive an antiparallel fashion of packing in order to cancel out each dipole.[5,6] As a result, an inversion center does occur in the crystal lattice of most molecular compounds conceived to present a NLO feature, which is responsible for vanishing the macroscopic second order polarizability from the crystal. However, several examples overcoming this undesirable crystal packing tendency from a NLO point of view are reported in the literature.[7]

As part of our continuous studies dealing with crystal engineering in molecular crystals, here we were concerned in planning a new promising NLO-exhibiting material invoking ground chemical principles for simple organic compounds. For this purpose, *trans*-1,2-bis(4-pyridyl)ethene (BPE), a well-known and straightforward molecule even without the intramolecular NLO requirement, was chosen for a crystal engineering strategy. This compound does not contain any π-electron acceptor group at one of its tails, even though there is a presence of π-electron donor pyridyl nitrogen and also π-electron delocalization encompassing its whole molecular backbone. To the best of our knowledge, BPE has been investigated as a ligand for transition metal ion complexes

[a] *Instituto de Química, Universidade Federal de Goiás, Campus Samambaia, CP 131, Goiânia, GO, 74001-970, Brazil. E-mail: felipe@ufg.br*
[b] *Instituto de Física, Universidade Federal de Goiás, Campus Samambaia, CP 131, Goiânia, GO, 74001-970, Brazil*
[c] *Instituto de Química Rosario (IQUIR), Universidad Nacional de Rosario–CONICET, Suipacha 531, S2002LRK Rosario, Argentina*

† CCDC 1489318. For crystallographic data in CIF or other electronic format see DOI: 10.1039/c6ce02229d

and cocrystals conceived for NLO applications,[8] but no NLO study on the crystal forms made up of only BPE, or of BPE together with crystallization matrix component(s) has been found in the literature thus far. We have here prepared a dihydrochloride salt dihydrate of BPE through the protonation of both pyridyl nitrogens using hydrochloric acid. The protonated form of BPE has crystallized in a non-centrosymmetric space group which was confirmed based on the second harmonic generation (SHG) from the crystals, since pseudo symmetry effects have introduced doubt on crystallization in a higher-symmetry centrosymmetric space group. In this study, we report the preparation, structural elucidation, DFT calculations and SHG signal of this organic salt dihydrate candidate for NLO application, together with the photoluminescence (PL) excitation and emission results for this multifunctional optical material.

Experimental

Preparation of the BPE dihydrochloride salt dihydrate

Firstly, a quantity of 2 mg of BPE (0.011 mmol) was dissolved in isopropyl alcohol (5 mL) under stirring for 5 min at room temperature (25 °C). In sequence, this solution was mixed with another solution of hydrochloric acid in water at a 0.28 mol L^{-1} concentration (0.25 ml, 0.07 mmol) under stirring (5 min, 25 °C). After slow evaporation of the resulting solution upon standing (15 days, 25 °C), needles were formed on the bottom and sides of the glass crystallizer. The totality of the synthesis and the crystal phase purity were confirmed through the powder X-ray diffraction technique after SHG measurement (Fig. 1).

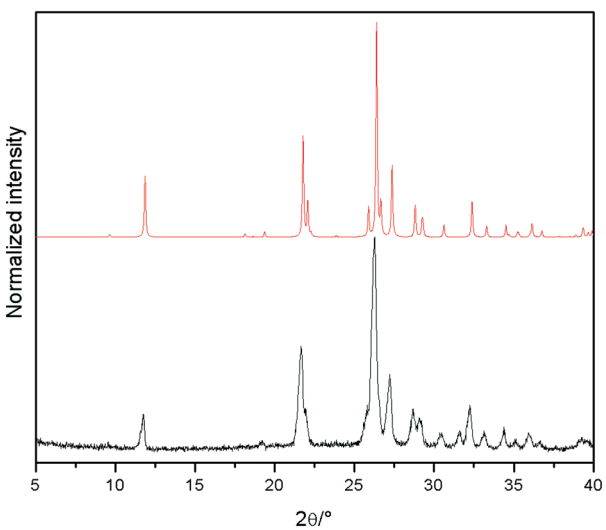

Fig. 1 Powder X-ray diffractograms of the BPE dihydrochloride salt dihydrate simulated from the single-crystal structure (red) and experimentally acquired (black). Intensity data were acquired at 298 K using graphite monochromatized CuKα radiation (λ = 0.15418 nm) generated at 40 kV and 30 mA on a Shimadzu XRD-6000 diffractometer (continuous θ–2θ scan mode with a scan speed of 1.000° min^{-1}, a collection step of 0.020°, divergence and scattering slits at 1.000°, and receiving slit at 0.300 mm).

Structure determination of BPE dihydrochloride salt dihydrate

A needle-shaped single crystal measuring 0.24 × 0.10 × 0.05 mm^3 was isolated from the glass crystallizer and mounted on a 100 μm loop (MiTeGen MicroLoops™). Next, the crystal was centered on the goniostat of a Bruker-AXS Kappa Duo diffractometer with an APEX II CCD detector. MoKα radiation from an IμS microsource with multilayer optics was employed for X-ray intensity collection at 23 °C. The diffraction frames were recorded by φ and ω scans using APEX2 software[9] for data collection strategy and frame acquisition. Raw dataset treatment including indexing, integrating, reducing and scaling of Bragg reflections was also performed using the program APEX2.[9] The structure was solved by direct methods with SHELXS-97,[10] wherein C, N, O and Cl were directly assigned from the electron density Fourier map. The initial model was refined by the full-matrix least squares method using F^2 with SHELXL-97.[10] Anisotropic and isotropic atomic displacement parameters were set for non-hydrogen and hydrogen atoms, respectively. Each hydrogen had its isotropic displacement parameter fixed [U_{iso}(H) = 1.2 U_{eq}(C or N) or 1.5 U_{eq}(O)]. Hydrogens bonded to carbons were positioned stereochemically with constrained C–H bond lengths of 0.93 Å following the riding model, while hydrogens bonded to water oxygens and protonated pyridyl nitrogen were doubtlessly assigned from the electron density difference Fourier map. The coordinates of water and N^+–H hydrogens were constrained after their assignment. In addition, the central double-bonded carbons were found to be disordered over two sets of 50% occupancy sites each. The programs MERCURY[11] and ORTEP-3 (ref. 12) were used within the WinGX[12] software package to prepare the artwork representations. CCDC reference number 1489318 contains the crystal data for the BPE dihydrochloride salt dihydrate in the space group *P*1 (Table 1).

SHG measurements of BPE dihydrochloride salt dihydrate

The second harmonic emission intensity of the crystals was evaluated by a Second Harmonic Generation (SHG) measurement setup. The 974 nm output of a CW diode laser (Crystalaser) operating at different powers was used as the pump beam. The crystals as obtained after slow solvent evaporation, *i.e.*, without either breaking or powdering them, were mounted in a random orientation onto a fixed mirror stage with an angle of 45° related to the pump beam, and the SHG signal was collected at reflectance configuration at 90° with respect to the pump beam using a double monochromator and a Hamamatsu photomultiplier tube, both integrated in the Fluorolog FL3-221 equipment (Horiba Jobin-Yvon). The signals around *ca.* 487 nm were collected by using emission slits of 2 nm, a time integration of 1 second, and increments of 0.2 nm.

Table 1 Crystal data and refinement statistics of the BPE dihydrochloride salt dihydrate [$(C_{12}H_{12}N_2)Cl_2(H_2O)_2$] in different space groups (data collection at 296 K using MoKα beam)

Space group	*P*1	*P*$\bar{1}$	*C*2	*Cm*	*C*2/*m*
a (Å)	4.75320(10)		18.3146(4)		
b (Å)	8.1538(2)		8.1538(2)		
c (Å)	10.0237(2)		4.75320(10)		
α (°)	113.9970(10)		90		
β (°)	91.2750(10)		91.3970(10)		
γ (°)	90.0030(10)		90		
V (Å^3)	354.801(13)		709.60(3)		
Z/*Z*′[a]	1/1	1/0.5	2/0.5	2/0.5	2/0.25
Unique reflections	2496	1438	1443	1349	774
Unique reflections with $I > 2\sigma(I)$	2261	1305	1312	1242	717
Symmetry factor (R_{int})	0.0341	0.0518	0.0526	0.0377	0.0542
Completeness to θ_{max} (%)/θ_{max} (°)	99.8/26.36		99.9/26.36		
F(000)	152		304		
Parameters refined	182	91	82	103	53
Goodness-of-fit on F^2	1.109	1.097	0.977	1.154	1.970
Final R_1 factor for $I > 2\sigma(I)$	0.0493	0.0691	0.0782	0.0675	0.1189
wR_2 factor for all data	0.1569	0.1836	0.2366	0.1818	0.3887
Largest diff. peak/hole (*e*/Å^3)	0.305/−0.286	0.366/−0.729	0.458/−0.608	0.379/−0.757	0.596/−1.626

[a] *Z* and *Z*′ numbers are relative to the $(C_{12}H_{12}N_2)Cl_2(H_2O)_2$ formula.

Theoretical calculations of NLO parameters

All calculations were performed using Gaussian 09.[13] The geometries of the single molecule and the cluster of four molecules were extracted from the crystal structure of the BPE dihydrochloride salt dihydrate. Firstly, prior to the electrical property calculation, two different strategies were carried out for the geometry optimization of the single-molecule. In one of them, the conformation found in the crystal was fully optimized without constraints (full optimization), while in the other one only the CH and NH bonds were optimized by freezing the coordinates of all C and N atoms (partial optimization). This last approach was employed for the four $\pi\cdots\pi$ stacked molecules. In all cases, the geometry optimizations were performed at the B3LYP/6-31G* level of theory. All the electrical properties were next computed at the CAM-B3LYP/NLO-V level of theory, using the B3LYP/6-31G* optimized geometries as inputs. The hybrid exchange-correlation functional CAM-B3LYP is the long-range corrected version of B3LYP that accounts for the true asymptotic behavior at long interelectronic distances.[14] NLO-V is a valence-double-zeta-polarized (VDZP) basis set that represents the augmented and re-contracted version of the Ahlrichs VDZ basis set, with radial exponents optimized for NLO calculations.[15] The combination of the CAM-B3LYP functional with the NLO-V basis set was found to provide satisfactory predictions of NLO properties of organic molecules.[15] The NLO-V basis set is not available in Gaussian 09, and was downloaded from http://bse.pnl.gov/bse/portal.

The average first hyperpolarizability values (β_{tot}) were calculated according to:

$$\beta_{tot} = \sqrt{\beta_x^2 + \beta_y^2 + \beta_z^2}$$

where the Cartesian β_x, β_y and β_z elements were calculated from the tensor elements β_{ijk}, according to:

$$\beta_i = \frac{1}{3}\sum\left(\beta_{ikk} + \beta_{kik} + \beta_{kki}\right) \forall k = x, y, z; i = x, y, z$$

The projection of β_{tot} in the dipole moment direction (β_{vec}) was computed according to:

$$\beta_{vec} = \sum_1^3 \frac{\mu_i \beta_i}{|\mu|}$$

PL excitation and emission measurements of BPE dihydrochloride salt dihydrate

PL excitation and emission spectra were recorded using a double monochromator and a Hamamatsu photomultiplier tube as the detector (Fluorolog FL3-221 from Horiba Jobin-Yvon), under excitations from a Xe arc lamp delivering 450 W. The bandpass was fixed at 1.0 nm, and each point was collected at each 1.0 nm. The emission color coordinates of the BPE crystals were determined using the experimental setup based on the PL emission spectra recorded by an integrating sphere and the software FluorEssence V3.5 integrated with the spectrofluorimeter (Fluorolog FL3-221, Horiba Jobin-Yvon). To measure the diffuse reflectance spectrum of the BPE dihydrochloride salt dihydrate, $BaSO_4$ powder was used as the reference material, and the spectrum was collected from 250 to 1400 nm. The absorption relates to the optical transition of electrons from the valence band to the conduction band and can be used to determine the character and values of the optical bandgap E_g of the crystals. Therefore, the optical bandgap of the sample was calculated on the

basis of the diffuse reflectance spectra using the equation:

$$F(R) = \frac{A(h\nu - E_g)^m}{h\nu}$$

where $F(R) = (1 - R)^2/(2R)$ is the Kubelka–Munk function,[16] R is the ratio between the diffuse reflectance from the sample and a reference material (in this study, $BaSO_4$), A is a constant, $h\nu$ is the incident photon energy, and m is 1/2 or 2 for undirected and direct transitions, respectively. Thus the value of the direct bandgap E_g for the crystal was obtained by extrapolating the linear part of the plot of $(F(R)h\nu)^2$ *versus* $h\nu$ to zero.

Results and discussion

Crystal structure

BPE is a weak NLO-phore in its neutral form due to the presence of two π-electron donor pyridyl nitrogens at the molecule tails hindering charge transfer along the molecular skeleton. Likewise, the protonation of both pyridyl nitrogens would give rise to a divalent cationic molecule with two π-electron acceptor iminium moieties with higher intramolecular charge transfer ability. Furthermore, intermolecular charge transfer occurs as a consequence of the face-to-tail stacking of protonated BPE molecules along the [100] direction through π···π interactions (Fig. 2). Such interactions are established between the donor π-electrons from the spacer double-bonded π-electron-rich carbons and the π-acceptor protonated electron-deficient pyridyl rings, which is possible due to the stacking of the translation-symmetry related molecules to have a slippage of 3.45 Å (Fig. 2). It is important to observe that such a face-to-tail stacking fashion does not result in a zigzag chain with alternating slippage directions. In the dihydrochloride salt dihydrate of BPE, the slippage in the stacking of BPE molecules occurs always towards the same direction as it occurs in the promising NLO crystal of *p*-nitrobenzylidene–*p*-phenylamineaniline.[17] This results in all chains of stacked molecules running in the same direction, with the intermolecular dipole-moment pointing towards the same direction and then avoiding their cancellation if otherwise they had been on opposite directions. Such a growth direction of the chains is another interesting crystal packing feature impacting on the SHG of our salt as it was already observed in the crystals of potential NLO materials.[6,17] Concerning the metrics of the key π···π interactions responsible for charge transfer here, the distances between the centroids calculated through C6 (or C6D) and C7 (or C7D) and through pyridyl rings A (N1, C1 to C5) and B (N2, C8 to C12) are 3.519(2) Å (or 3.547(2) Å) and 3.500(2) Å (or 3.472(2) Å),

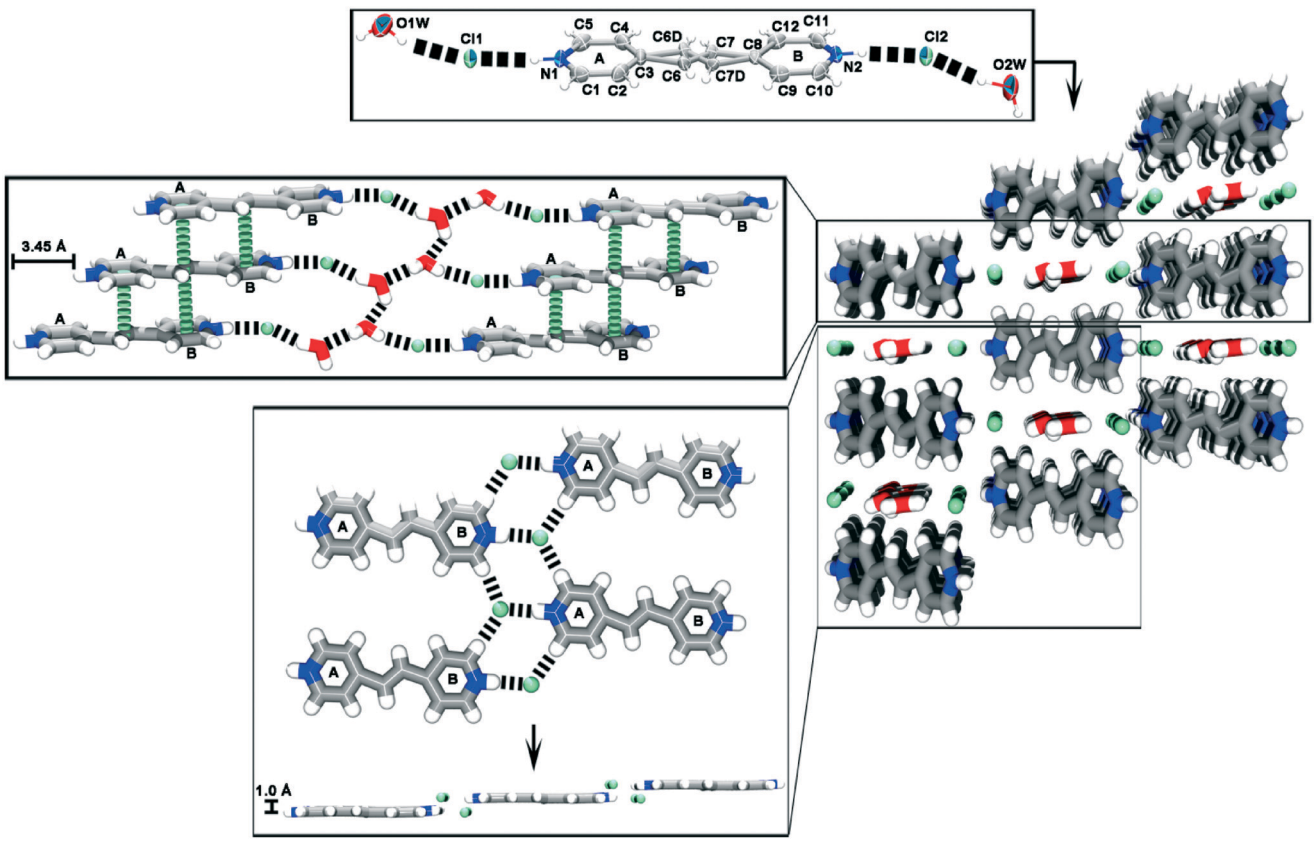

Fig. 2 A view of the crystal structure of the BPE dihydrochloride salt dihydrate (right) and insets of the asymmetric unit (top; non-hydrogen atoms as 30% probability ellipsoids) and supramolecular chains (hydrogen bonds and π···π interactions are shown as dashed black and green lines, respectively).

respectively, without a stacking bend angle. Such interactions are significantly energetic and therefore favoured due to the fact that the acceptor π-cloud is positively polarized as in the case of our crystal form of BPE present with one net positive charge at each pyridyl ring.

The two chloride anions and the divalent cation of BPE found in the non-centrosymmetric triclinic unit cell are hydrogen bonded through N^+–H···Cl^-, forming a planar neutral building block (BPE)Cl_2, with a RMSD value calculated for the least square plane crossing through its sixteen non hydrogen atoms of 0.0298 Å if calculated with C6 and C7 or 0.0327 Å if calculated with C6D and C7D. There are no significant differences in the hydrogen bonding geometric parameters of the two crystallographically independent N^+–H··· Cl^- hydrogen bonds which could reflect a noteworthy dipole moment through the (BPE)Cl_2 bluing block, except for the angle of the interactions slightly differing by 3° (Table 2). These building blocks are packed side-to-side and head-to-head into a two-dimensional sheet through nonclassical C–H···Cl^- bonds involving the two CH moieties at 3 and 5 positions of both pyridyl rings and chloride counterions from neighboring building blocks. Whether the (BPE)Cl_2 units are packed side-to-side through these interactions, they form a planar chain. Each planar chain is further packed head-to-head to another one, with a rise of 1.0 Å (Fig. 2).

Water molecules play an important role in the crystal assembly of the dihydrochloride salt dihydrate (Fig. 2). They form a hydrogen bonded wire growing along the [100] direction. In these wires, each crystallographically independent water molecule is a hydrogen bond donor to the oxygen of another one. The other hydrogen of each water molecule is engaged in hydrogen bonding with chloride anions of stacked building blocks. However, one water molecule is a hydrogen bond donor to chloride interacting with pyridyl, while the other crystallographically independent water is hydrogen bonded to chloride connected to pyridyl ring B. Consequently, these two water molecules are alternated into the wires to interact with stacked building blocks forming chains packed onto the (100) plane (Fig. 2).

We have evaluated the presence of higher symmetry in the crystal structure of the dihydrochloride salt dihydrate of BPE. Symmetry elements of the *C*-centered monoclinic setting (space group *C*2/*m*) were found using PLATON.[18] We have thus checked carefully the systematic extinctions. Neither reflection has violated the systematic extinction condition for the presence of the *C*-centering, *i.e.*, no reflection with an odd $(h + k)$ sum was observed (mean Int./σInt. < 2.0). The structure was then solved and refined in all *C*2, *Cm* and *C*2/*m* space groups, but the outputted refinement statistics were worse than those outputted by the refinement in the *P*1 space group, as can be viewed in Table 1. Besides that, geometry faults in the open-chain and non-definite positive ellipsoids were observed if refined in *C*2 and *Cm* space groups, respectively. Furthermore, the presence of inversion symmetry as occurs in the refined *C*2/*m* and *P*$\bar{1}$ space groups was excluded through SHG by the BPE dihydrochloride salt dihydrate crystals, which have also yielded statistical parameters worse than those from refinement in *P*1. Therefore, we concluded this to be a typical pseudo centrosymmetric case besides a pseudo *C*-centered lattice with odd $(h + k)$ sum reflections being systematically weak but not absent. Despite that SHG is typically observed in noncentrosymmetric materials,[19] however, a few compounds can be solved in centrosymmetric space groups with residual non-centrosymmetry concluded

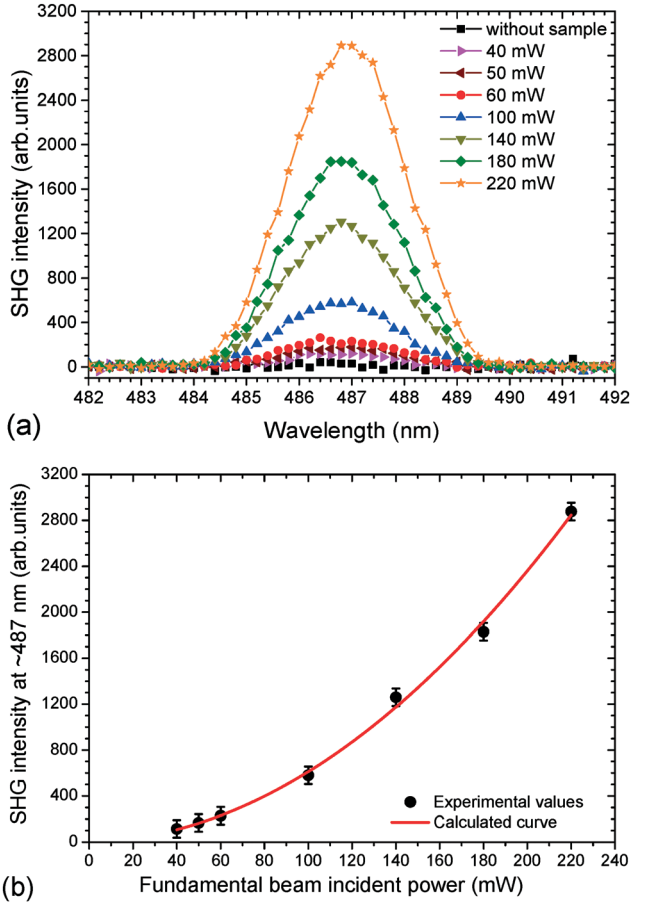

Fig. 3 (a) SHG emission spectra of BPE dihydrochloride salt dihydrate crystals, excited by a CW diode laser operating at ~974 nm with different powers. (b) SHG intensity values at ~487 nm as a function of the CW diode laser power and a calculated curve from a quadratic function (red line).

Table 2 Geometry of intermolecular hydrogen bonds in the BPE dihydrochloride salt dihydrate (distances in Å and angles in °)

Motifs	D–H···A	D–H	H···A	D···A	D–H···A
Py^+–Cl^-	N1P–H1P···Cl1	0.86	2.15	3.008(6)	176
	N2P–H2P···Cl2	0.86	2.15	3.006(6)	173
	C1–H1···Cl2	0.93	2.67	3.545(9)	158
	C5–H5···Cl2	0.93	2.68	3.552(9)	157
	C10–H10···Cl1	0.93	2.67	3.543(9)	157
	C11–H11···Cl1	0.93	2.67	3.546(9)	158
Water–Cl^-	O1W–H1W···Cl1	0.84	2.37	3.126(8)	150
	O2W–H3W···Cl2	0.99	2.16	3.120(8)	162
Water–water	O1W–H2W···O2W	0.85	2.01	2.641(9)	130
	O2W–H4W···O1W	0.99	1.90	2.632(9)	129

from SHG, as occurs in the complex $[Zn_2(benzoate)_4(4\text{-styrylpyridine})_2]$.[20] This complex has been successfully refined in the *C*2/*c* space group despite the presence of SHG. In this structure, a true crystallographic inversion centre is found in the middle of the paddle wheel shaped discrete coordination complex molecule. The observed large second-order nonlinearity is attributed to a small excess of polarity packing there. In our structure, there is polarity in the BPE^{2+} molecular backbone as well as in its packing, as can be seen in sequence in the theoretical NLO parameters. This study then reinforces the importance of assessing if a higher symmetry is in fact in the crystal lattice, since important properties depending on the absence of centrosymmetry, such as NLO, can even be neglected in an early stage of screening for these materials upon forcing a crystal to assume symmetry that it only appears to have.

Experimental SHG

Fig. 3 illustrates the SHG signal centered at *ca.* 487 nm of the BPE dihydrochloride salt dihydrate crystals. For these measurements, different powers delivered by a CW diode laser emitting at ~974 nm were used. To confirm that the second harmonic of the laser was not present, a measurement was made using only the mirror (without sample), and, as expected, no signal was detected. Fig. 3(a) shows the dependence of the SHG intensity (~487 nm) on the fundamental beam (~974 nm) incident power ranging between 40 mW and 220 mW. In fact, upon increasing the laser power onto the BPE dihydrochloride salt dihydrate crystals, the sample SHG signal presents a high increase. A best fitting was performed from a quadratic function, Fig. 3(b) (straight red line), and a good adjusted *R*-square of 0.99823 was obtained. This quadratic behavior agrees well with nonlinear optical theory prediction,[21] and, in the studied laser power range of 40–220 mW, we have not detected a saturation effect at higher powers, considering that each point of the spectra was collected for 1 second. Our results suggest that these new BPE dihydrochloride salt dihydrate crystals are suitable for small size devices which require nonlinear optical properties, such as microlasers, for example. We have also attempted to measure SHG from the powder sample obtained after grinding the crystals, but no SHG intensity was acquired with the same experimental optical setup used for the crystals before powdering them. Such SHG quenching through powdering larger crystals was also observed in the centrosymmetric complex $[Zn_2(benzoate)_4(4\text{-styrylpyridine})_2]$ present with residual non-centrosymmetry.[20]

Theoretical insights into second-order nonlinearity

In addition to the SHG measurement, we have also analyzed theoretically the microscopic NLO response of BPE in its fully protonated form as found in the dihydrochloride salt dihydrate. The dipole moment (μ), average polarizability (α), average first hyperpolarizability (β_{tot}) and projection in the dipole-moment direction (β_{vec}) with a static field ($\omega = 0$) were estimated, at the CAM-B3LYP/NLO-V// level of theory, for single and four-molecules (Table 3).

Full optimization has converged to a twisted BPE cation, with an angle between the pyridyl planes of *ca.* 16°, while partial optimization has outputted a planar molecule resembling the crystal conformation as a consequence of freezing all C–C and C–N bonds during geometrical optimization. The fully optimized molecule had almost null μ, β_{tot} and β_{vec}, which reflects its non-polarity. However, these values differ from zero in the crystal conformation (partial optimization), revealing a molecular polarity gain upon crystallization in the dihydrochloride salt dihydrate. More interestingly, a *ca.* 4-fold increase in the main NLO descriptor β_{tot} and also in α and μ was observed for the tetramer of $\mathbf{1}^{2+}$, reflecting the polar stacking fashion of four molecules by means of $\pi\cdots\pi$ interactions.

Face-to-tail stacking is responsible for pointing the intermolecular charge transfer (CT) direction (see below) of all molecules in the same direction, resulting in a large increase in the microscopic theoretical NLO parameters which are proportional to the number of packed molecules. Here, it is important to take into account that all $\pi\cdots\pi$ stacked chains grow in the same direction, *i.e.*, they are not inverted in the crystal lattice, which would cancel intermolecularly the CT. Such a CT orientation does not occur in centrosymmetric crystals featuring face-to-face molecular stacking, wherein each molecule is antiparallel-pillared on each other, thus cancelling the overall macroscopic CT.[6] Likewise, intramolecular CT also occurs in the crystal conformation. This can be derived from the two-state model,[22] where the CT contribution to the overall first hyperpolarizability, namely, β_{CT}, prevails. The β_{CT} is related to the transition features from the ground state (g) to the excited state (e), being proportional to the

Table 3 Dipole moment (μ), average polarizability (α), average first hyperpolarizability (β_{tot}), and its projection in the dipole moment direction (β_{vec}) (static field) calculated for the fully protonated form of BPB

Input	μ (Debye)	α (10^{-23} esu)	β_{tot} (10^{-30} esu)	β_{vec} (10^{-30} esu)
BPE^{2+a}	0.15	2.20	3.56	2.63
BPE^{2+b}	0.08	2.42	0.0013	0.0010
4 $BPE^{2+a,c}$	0.58	8.35	12.55	4.67

[a] The conformation found in the dihydrochloride salt dihydrate has been inputted in the calculations, but only the CH and NH bonds were optimized at the B3LYP/6-31G* level of theory before extracting the shown NLO parameters at the CAM-B3LYP/NLOV// level. [b] Contrary to the previous footnote, all bonds were fully optimized. [c] The four molecules are $\pi\cdots\pi$ stacked neighbors as shown in Fig. 2.

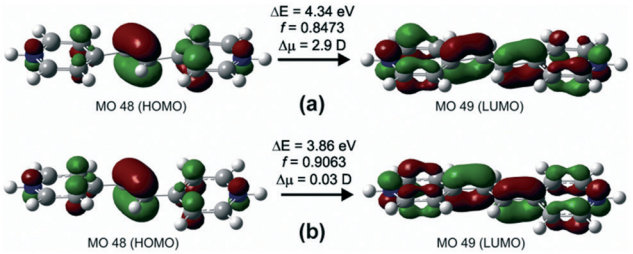

Fig. 4 Molecular orbitals involved in the charge transfer transition calculated at the CAM-B3LYP/NLOV// level by optimizing either only (a) C–H and N–H bonds (partial optimization) or (b) all bonds (full optimization) at the B3LYP/6-31G* level of theory. HOMO and LUMO represent the ground and excited states, respectively. *f*, ΔE and $\Delta\mu$ denote the oscillator strength, transition energy and the change in dipole moment upon excitation, respectively.

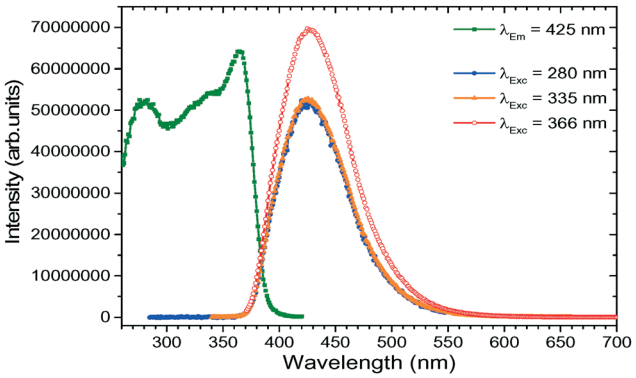

Fig. 5 Photoluminescence excitation and emission spectra of BPE dihydrochloride salt dihydrate crystals.

$(f\ \Delta\mu)/\Delta E^3$ ratio, wherein *f*, ΔE and $\Delta\mu$ are the oscillator strength, transition energy and the change in dipole moment upon excitation. Substituting into this expression the values given in Fig. 4, where the main molecular orbitals (MOs) of the two electronic states involved in the intramolecular CT transition are shown, β_{CT} values of 5×10^{-4} and 298×10^{-4} D eV^{-3} were calculated for the fully and partially optimized single molecules, respectively. These values are in agreement with the corresponding β_{tot} values shown in Table 3 (0.0013×10^{-30} esu and 3.56×10^{-30} esu for full and partial optimizations, respectively). Therefore, intramolecular CT contributes to the NLO response of the dihydrochloride salt dihydrate of BPE. This should also be the case for the packed four-molecules; however, the two-state model is not enough to assess the individual contributions to the NLO response, because the transitions have contributions from several excitation levels and they do not allow ascertaining precisely the CT.[22] Even so, intermolecular CT is found in the face-to-tail π···π stacked four-molecules (Fig. 2). Such an interaction is supported on the distribution of the main MOs. The HOMO orbital is mainly located over the double-bonded carbons C6 and C7, while LUMO is mostly distributed over their neighboring single bonds and pyridyl rings from two stacked molecules.

Photoluminescence emission measurements

In Fig. 5, the photoluminescence (PL) excitation and emission spectra of BPE dihydrochloride salt dihydrate crystals are presented. The excitation spectrum was acquired monitoring the emission at 425 nm, which was the only emission band observed. Also, emission spectra are shown for excitations at 280, 335 and 366 nm wavelengths (4.43 eV, 3.70 eV, and 3.39 eV respectively). Three bands between 270 and 370 nm are observed in the excitation photoluminescence spectra, which led to a broad band emission between 370 nm and 550 nm (ultraviolet, violet, blue and green emissions), with the maximum at 425 nm (2.91 eV). This PL emission can be related to the LUMO to HOMO transition and some energy lost to vibrational oscillations. Note in Fig. 4(b) that the energy difference between LUMO and HOMO is 3.86 eV, being close to the excitation band centre at 3.70 eV (335 nm). However, the highest emission occurs for the excitation in the lowest energy band at 3.39 eV (366 nm), and probably the excited levels are coupled to the phonon modes of the crystal. This broad band emission of BPE dihydrochloride salt dihydrate crystals seems to be useful for optical applications in OLEDs, such as light emitters.

Fig. 6 shows the colorimetric coordinates (x = 0.22 and y = 0.16, closed blue circle) of our crystal, being closer to blue color (x = 0.17 and y = 0.00), but shifted to standard white color (x = 0.33 and y = 0.33, open circle in Fig. 6), characterizing thus a cold-white PL emission. This bluish emission color is desired for solid state lighting (SSL) applications.

The diffuse reflectance spectrum of BPE dihydrochloride salt dihydrate crystals is illustrated in Fig. 7, with its strong optical bandgap absorption around 379 nm. In fact, the material absorbs from 600 nm to 250 nm, but the highest absorption occurs between 425 nm and 250 nm. As shown in Fig. 7, the direct bandgap E_g for the crystal is 3.27 eV. This E_g value is smaller than that calculated and shown above (3.86

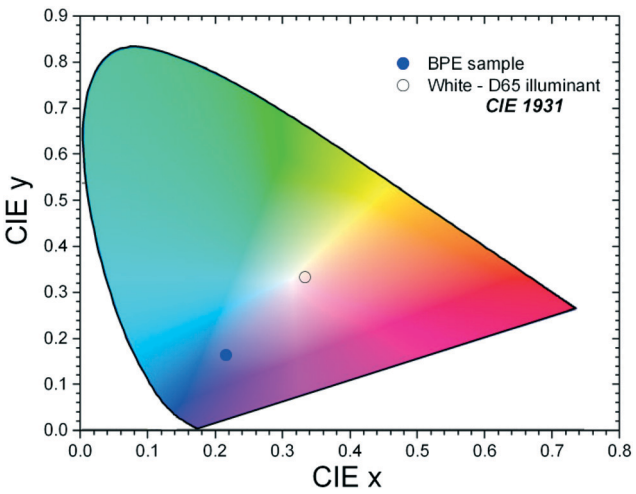

Fig. 6 CIE 1931 color coordinates of the PL emission from BPE dihydrochloride salt dihydrate crystals.

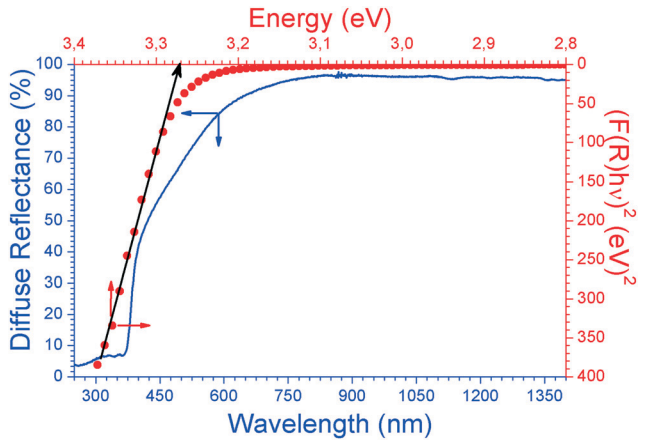

Fig. 7 Diffuse reflectance spectrum of BPE dihydrochloride salt dihydrate crystals from 250 to 1400 nm, and its bandgap determination.

eV). It may be due to the fact that this calculated E_g took into account a fully-optimized molecule and did not consider any lattice defect or environment which could have introduced new electronic levels inside the crystal bandgap.

Conclusions

Here we have prepared a new NLO material from the well-known BPE invoking the fundamental acid–base concept. Its synthesis is practical, easy and rapid, requiring only one step, besides presenting low cost and 100% yield. It is characterized by the presence of a planar hydrogen bonded building block $(BPE)Cl_2$ and two water molecules in the triclinic unit cell. The protonated BPE molecules are stacked face-to-tail along the [100] direction through π···π interactions. Such interactions are established between the donor π-electrons from the spacer double-bonded carbons and the acceptor protonated pyridyl ring. Furthermore, there is a slippage of 3.45 Å in the stacking of BPE cations always stacked towards the same direction, which is found commonly in other NLO crystals. Even though its crystal structure has been solved and refined in the space group *P*1, this material has a pseudo centrosymmetry. However, SHG measurements and theoretical NLO parameters, calculated at the CAM-B3LYP/NLO-V//B3LYP/6-31G* level of theory for the crystal conformation and its aggregate, have confirmed the absence of a true inversion centre in the structure. When compared to one single BPE cation in its locked crystal conformation, there was a *ca.* 4-fold increase in the main NLO descriptor β_{tot}, as well as in α and μ for the molecular cluster made up of four π···π stacked BPE cations. Therefore, such a face-to-tail stacking fashion through π···π interactions between the π-electron rich double-bonded carbons and the π-acceptor protonated pyridyl ring has been responsible for the magnification of the first hyperpolarizability and thus the found macroscopic NLO response. On the other hand, μ, β_{tot}, β_{CT} and β_{vec} did not deviate significantly from zero for the gas phase BPE cation. Therefore, the dihydrochloride sat dihydrate form of the long-time studied BPE is a promising candidate for NLO applications. Also, this new NLO material presents a broad band photoluminescence emission with a maximum at 425 nm, having the highest emission intensity for 366 nm excitation. It is a smart optical material with dual functionality which can be tuned according to need in optical devices.

Acknowledgements

The authors acknowledge CNPq, CAPES, and FAPEG for financial support and research fellowships (LJQM and FTM).

Notes and references

1 (*a*) P. J. Tejkiran, M. S. B. Teja, P. S. S. Kumar, P. Sankar, R. Philip, S. Naveen, N. K. Lokanath and G. N. Rao, *J. Photochem. Photobiol., A*, 2016, **324**, 33; (*b*) R. Tang, S. Zhou, W. Xiang, Y. Xie, H. Chen, Q. Peng, G. Yu, B. Liu, H. Zeng, Q. Li and Z. Li, *J. Mater. Chem. C*, 2015, **3**, 4545; (*c*) M. Fedoseeva, P. Fita, A. Punzi and E. Vauthey, *J. Phys. Chem. C*, 2010, **114**, 13774; (*d*) A. Bossi, E. Licandro, S. Maiorana, C. Rigamonti, S. Righetto, G. R. Stephenson, M. Spassova, E. Botek and B. Champagne, *J. Phys. Chem. C*, 2008, **112**, 7900; (*e*) O. R. Evans and W. B. Lin, *Acc. Chem. Res.*, 2002, **35**, 511.

2 (*a*) W. Jin, P. V. Johnston, D. L. Elder, K. T. Manner, K. E. Garrett, W. Kaminsky, R. Xu, B. H. Robinson and L. R. Dalton, *J. Mater. Chem. C*, 2016, **4**, 3119; (*b*) G. Martin-Gassin, G. Arrachart, P.-M. Gassin, N. Lascoux, I. Russier-Antoine, C. Jonin, E. Benichou, S. Pellet-Rostaing, O. Diat and P.-F. Brevet, *J. Phys. Chem. C*, 2012, **116**, 7450; (*c*) S. R. Marder, L.-T. Cheng, B. G. Tiemann, A. C. Friedli, M. Blanchard-Desce, J. W. Perry and J. Skindhøj, *Science*, 1994, **263**, 511.

3 (*a*) C. Botta, E. Cariati, G. Cavallo, V. Dichiarante, A. Forni, P. Metrangolo, T. Pilati, G. Resnati, S. Righetto, G. Terraneo and E. Tordin, *J. Mater. Chem. C*, 2014, **2**, 5275; (*b*) S. Draguta, M. S. Fonari, A. E. Masunov, J. Zazueta, S. Sullivan, M. Y. Antipin and T. V. Timofeeva, *CrystEngComm*, 2013, **15**, 4700; (*c*) T. V. Timofeeva, V. N. Nesterov, R. D. Clark, B. Penn, D. Frazier and M. Y. Antipin, *J. Mol. Struct.*, 2003, **647**, 181.

4 (*a*) K. Feng, L. Kang, Z. Lin, J. Yao and Y. Wu, *J. Mater. Chem. C*, 2014, **2**, 4590; (*b*) D. Lumpi, F. Gloecklhofer, B. Holzer, B. Stoeger, C. Hametner, G. A. Reider and J. Froehlich, *Cryst. Growth Des.*, 2014, **14**, 1018.

5 (*a*) M. O. Senge, M. Fazekas, E. G. A. Notaras, W. J. Blau, M. Zawadzka, O. B. Locos and E. M. N. Mhuircheartaigh, *Adv. Mater.*, 2007, **19**, 2737; (*b*) Y. Liao, S. Bhattacharjee, K. A. Firestone, B. E. Eichinger, R. Paranji, C. A. Anderson, B. H. Robinson, P. J. Reid and L. R. Dalton, *J. Am. Chem. Soc.*, 2006, **128**, 6847; (*c*) M. J. G. Lesley, A. Woodward, N. J. Taylor, T. B. Marder, A. Thornton, D. W. Bruce and A. K. Kakkar, *Chem. Mater.*, 1998, **10**, 1355.

6 (*a*) K. Y. Suponitsky and A. E. Masunov, *J. Chem. Phys.*, 2013, **139**, 094310; (*b*) J. M. Cole, J. A. K. Howard and G. J. McIntyre, *Acta Crystallogr., Sect. B: Struct. Sci.*, 2001, **57**, 410.

7 (*a*) G. Yang, G. Peng, N. Ye, J. Wang, M. Luo, T. Yan and Y.

Zhou, *Chem. Mater.*, 2015, **27**, 7520; (*b*) Y. Song, C.-S. Lin, M.-J. Zhang, Q. Wei, M.-L. Feng and X.-Y. Huang, *CrystEngComm*, 2015, **17**, 3418; (*c*) Z. Sun, X. Liu, X. Wang, L. Li, X. Shi, S. Li, C. Ji, J. Luo and M. Hong, *Cryst. Growth Des.*, 2012, **12**, 6181; (*d*) M. Sliwa, S. Letard, I. Malfant, M. Nierlich, P. G. Lacroix, T. Asahi, H. Masuhara, P. Yu and K. Nakatani, *Chem. Mater.*, 2005, **17**, 4727; (*e*) O. R. Evans and W. B. Lin, *Chem. Mater.*, 2001, **13**, 2705.

8 (*a*) W. Zhu, R. Zheng, X. Fu, H. Fu, Q. Shi, Y. Zhen, H. Dong and W. Hu, *Angew. Chem., Int. Ed.*, 2015, **54**, 6785; (*b*) C. Xu, Z.-Y. Zhang, Z.-G. Ren, L.-K. Zhou, H.-X. Li, H.-F. Wang, Z.-R. Sun and J.-P. Lang, *Cryst. Growth Des.*, 2013, **13**, 2530; (*c*) C. Zhang, Y. Cao, J. Zhang, S. Meng, T. Matsumoto, Y. Song, J. Ma, Z. Chen, K. Tatsumi and M. G. Humphrey, *Adv. Mater.*, 2008, **20**, 1870; (*d*) J. Li, Y. Song, H. Hou, M. Tang, Y. Fan and Y. Zhu, *J. Organomet. Chem.*, 2007, **692**, 158; (*e*) M. Pizzotti, R. Ugo, D. Roberto, S. Bruni, P. Fantucci and C. Rovizzi, *Organometallics*, 2002, **21**, 5830.

9 *APEX2*, Bruker AXS Inc., Madison, Wisconsin, USA, 2009.

10 G. M. Sheldrick, *Acta Crystallogr., Sect. A: Found. Crystallogr.*, 2008, **64**, 112–122.

11 C. F. Macrae, I. J. Bruno, J. A. Chisholm, P. R. Edgington, P. Mccabe, E. Pidcock, L. R. Monge, R. Taylor, J. van de Streek and P. A. Wood, *J. Appl. Crystallogr.*, 2008, **41**, 466.

12 L. J. Farrugia, *J. Appl. Crystallogr.*, 2012, **45**, 849.

13 M. J. Frisch, G. W. Trucks, H. B. Schlegel, G. E. Scuseria, M. A. Robb, J. R. Cheeseman, G. Scalmani, V. Barone, B. Mennucci, G. A. Petersson, H. Nakatsuji, M. Caricato, X. Li, H. P. Hratchian, A. F. Izmaylov, J. Bloino, G. Zheng, J. L. Sonnenberg, M. Hada, M. Ehara, K. Toyota, R. Fukuda, J. Hasegawa, M. Ishida, T. Nakajima, Y. Honda, O. Kitao, H. Nakai, T. Vreven, J. A. Montgomery Jr., J. E. Peralta, F. Ogliaro, M. Bearpark, J. J. Heyd, E. Brothers, K. N. Kudin, V. N. Staroverov, R. Kobayashi, J. Normand, K. Raghavachari, A. Rendell, J. C. Burant, S. S. Iyengar, J. Tomasi, M. Cossi, N. Rega, J. M. Millam, M. Klene, J. E. Knox, J. B. Cross, V. Bakken, C. Adamo, J. Jaramillo, R. Gomperts, R. E. Stratmann, O. Yazyev, A. J. Austin, R. Cammi, C. Pomelli, J. W. Ochterski, R. L. Martin, K. Morokuma, V. G. Zakrzewski, G. A. Voth, P. Salvador, J. J. Dannenberg, S. Dapprich, A. D. Daniels, O. Farkas, J. B. Foresman, J. V. Ortiz, J. Cioslowski and D. J. Fox, *Gaussian 09*, Gaussian, Inc., Wallingford CT, 2009.

14 T. Yanai, D. P. Tew and N. C. Handy, *Chem. Phys. Lett.*, 2004, **393**, 51.

15 D. Paschoal and H. F. dos Santos, *J. Mol. Model.*, 2013, **19**, 2079.

16 P. Kubelka and F. Z. Munk, *Tech. Phys.*, 1931, **12**, 593.

17 T. E. Souza, I. M. L. Rosa, A. O. Legendre, D. Paschoal, L. J. Q. Maia, H. F. dos Santos, F. T. Martins and A. C. Doriguetto, *Acta Crystallogr., Sect. B: Struct. Sci., Cryst. Eng. Mater.*, 2015, **71**, 416.

18 A. L. Spek, *J. Appl. Crystallogr.*, 2003, **36**, 7.

19 W. G. Cady, *Piezoelectricity*, McGraw-Hill, New York, 1946.

20 V. Nalla, R. Medishetty, Y. Wang, Z. Bai, H. Sun, J. Wei and J. J. Vittal, *IUCrJ*, 2015, **2**, 317.

21 R. W. Boyd, *Nonlinear Optics*, Elsevier, New York, 3th edn, 2007.

22 (*a*) A. Willetts, J. E. Rice, D. M. Burland and D. P. Shelton, *J. Chem. Phys.*, 1992, **97**, 7590; (*b*) J. L. Oudar and D. S. Chemla, *J. Chem. Phys.*, 1977, **16**, 1179; (*c*) J. L. Oudar, *J. Chem. Phys.*, 1977, **77**, 446.

